SERIES

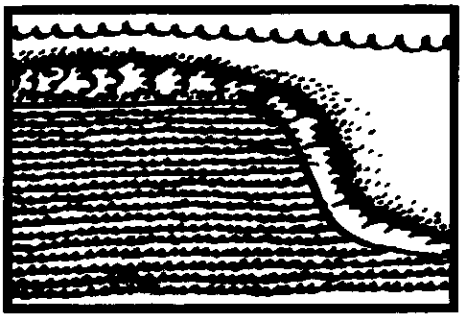

Environmental Marine Geoscience 4.

Continental Shelf Sediment Transport Studies in Canada: Principal Scientific Advances and Future Directions

Michael Z. Li and Dave E. Heffler
Geological Survey of Canada (Atlantic)
Bedford Institute of Oceanography
Dartmouth, Nova Scotia B2Y 4A2
mli@NRCan.gc.ca

SUMMARY
This article, the second of two companion papers, reviews the principal scientific advances in shelf sediment transport studies in Canada, and projects future research directions. Development of new sensors and boundary layer models has led to significant improvement in our understanding of wave-current dynamics and sediment transport processes on continental shelves. Bed shear stress and bottom roughness are found to be strongly enhanced by the interaction between waves and currents. Explicit sediment transport thresholds and ripple predictors for combined waves and currents have been proposed and partly tested. Sand resuspension strongly depends on the development of bedforms. Multibeam mapping, in combination with coring and seismic/sidescan data, has significantly improved our knowledge of the morphology and stability of sand ridges on outer-shelf sand banks. Sediment transport models have been significantly upgraded and calibrated based on advances in combined-flow bottom boundary layer dynamics and new *in situ* measurements of sediment transport. The improved models have been applied to predict regional sediment transport patterns on several Canadian continental shelves. Based on this and other reviews, future research priorities have also been identified.

RÉSUMÉ
Dans cet article, le second de deux sur le sujet, on décrit les principales percées scientifiques dans le domaine du transport des sédiments côtiers au Canada ainsi que des pistes de recherches à venir. La mise au point de nouveaux capteurs et de nouveaux modèles sur les couches limites a considérablement amélioré nos connaissances sur les interactions vagues-courants ainsi que sur les processus de transport des sédiments sur les plateaux continentaux. On s'est rendu compte que la contrainte de cisaillement ainsi que l'accentuation du relief du fond sont fortement tributaires de l'action combinée des vagues et des courants. Des seuils de mise en mouvement ainsi que des prédicteurs de formation de ride liés à des combinaisons de vagues-courants particuliers ont fait l'objet de tests partiels. La remise en suspension du sable est fonction de la configuration des lits. L'utilisation de la cartographie à faisceaux multiples et des données de forages combinés avec les données de levées sismiques et de sonar latéral a permis d'améliorer considérablement nos connaissances sur la morphologie et la stabilité des crêtes des bancs de sables de la partie extérieure du talus continental. Les modèles de transport des sédiments ont été considérablement améliorés et calibrés grâce à des découvertes dans le domaine de la dynamique des flux combinés des couches limites sur les fonds marins ainsi que par de nouvelles mesures in situ du transport des sédiments. Ces modèles améliorés ont été utilisés comme outils de prédiction des caractéristiques régionales du transport des sédiments en plusieurs endroits du plateau continental canadien. Aussi, à partir de la présente revue et d'autres, des pistes de recherche prioritaires ont été décrites.

INTRODUCTION

Sediment transport on continental shelves involves complex processes of sediment erosion, transport, and deposition close to the seabed. Since these processes can greatly affect seabed stability, the dispersal and deposition of sediment particles, and the activities of benthic organisms, shelf sediment transport studies have become increasingly important to oceanographers and coastal engineers as well as environmental managers (Grant and Madsen, 1986; Wright, 1989; Cacchione and Drake, 1990; Nittrouer and Wright, 1994).

This article and an earlier companion article (Li and Heffler, 2002) intend to provide an overview of the status and advances of shelf sediment transport research in Canada. A more comprehensive introduction to the topic has been given in the earlier paper, which presents the basic theories of shelf sediment transport, a quick review of the state of knowledge until the late 1980s, and recent technological advances in this research field. As a companion paper, the focus of this article is on the principal

scientific advances in the last 15 years and the projection of future research directions. While most studies presented in this paper deal with advances of sand transport on continental shelves, scientists in the United States recently have undertaken a program (STRATAFORM) that focusses on the transport and deposition of fine-grained sediment on the California shelf (Nittrouer, 1999).

PRINCIPAL SCIENTIFIC ADVANCES

Earlier reviews of shelf sediment transport studies in Canada (*e.g.,* Hodgins *et al.*, 1986) identified several critical areas that should receive priority for further research. These include better understanding of the boundary layer dynamics under combined waves and currents, determining the threshold of sediment motion under combined-flow conditions, bedform development and interaction with nearbed waves and currents, and obtaining comprehensive field data on wave-current dynamics and sediment transport. Development of new sensors and modelling technologies in recent years (as reviewed in Li and Heffler, 2002) has led to progress in some of these research areas. A comprehensive field program has been undertaken by the Geological Survey of Canada–Atlantic (GSCA) since the early 1990s to study wave-current dynamics and sediment transport during storms on Sable Island Bank (SIB), Scotian Shelf. The results from this program will be used as the focus to demonstrate the principal scientific advances in Canadian shelf sediment transport studies.

Boundary Layer Dynamics Under Combined Waves and Currents

Enhancement of Bed Shear Stress and Bottom Roughness Due to Wave-current Interaction

The large errors and differences in the predictions of available sediment transport models are, to a large extent, due to the inclusion of many empirical coefficients and the lack of a proper physical understanding of the boundary layer processes involved (Hodgins *et al.*, 1986). The solution lies in better understanding of boundary layer processes and hence better parameterization of the bottom stresses and their influence on sediment transport. The development of combined-flow bottom boundary layer (bbl) models (*e.g.,* Smith, 1977; Grant and Madsen, 1979, 1986) represented a breakthrough in our understanding of boundary layer processes. However, field measurements of wave-current dynamics and seabed roughness in diverse shelf and nearshore environments are still required to test and improve these models (Cacchione and Drake, 1990). With this as one of the objectives, the Geological Survey of Canada (GSC) instrumented tripod RALPH was deployed at a site about 60 km to the southwest of Sable Island (Site 1, Fig. 1) in the winter of 1992-1993 to monitor nearbed waves, currents, and seabed response during storms. The water depth at this site was 39 m and the bottom sediment was well-sorted medium sand with a mean grain size of 0.34 mm.

The water depth time series in Fig. 2a clearly shows the semidiurnal tidal oscillation in the study region. One neap tide and two spring tides occurred during the experiment. The tide range was 0.5 m during the neap tide and increased to 1.5 m during the spring tide. The peak mean (mainly tidal) current velocity was around 0.35 m/s (Fig. 2b) and the mean current direction was to the N and NE, or S and SW. Three storms occurred during the experiment, with significant wave heights from 2.5 m to 4 m and spectral peak wave periods from 12 s to 15 s (Fig. 2c). The time series of the suspended sediment concentration in Fig. 2d shows three suspension events (at the beginning, the 12th day and the end of the deployment). These corresponded with the passing of the three storms.

The wave and current parameters in Figure 2, together with the grain size and water depth data, were used in the Grant and Madsen (1986, GM86 hereafter) combined-flow boundary layer model to compute various bbl parameters, and these were then compared to observed seabed responses to further our understanding of combined-flow boundary layer processes. The mean velocity at 1 m above the seabed u_{100} and its drag coefficient C_{100} = 0.003 (for rippled sand bed, Sternberg, 1972) were used in a quadratic stress law (eq. 3 in Li and

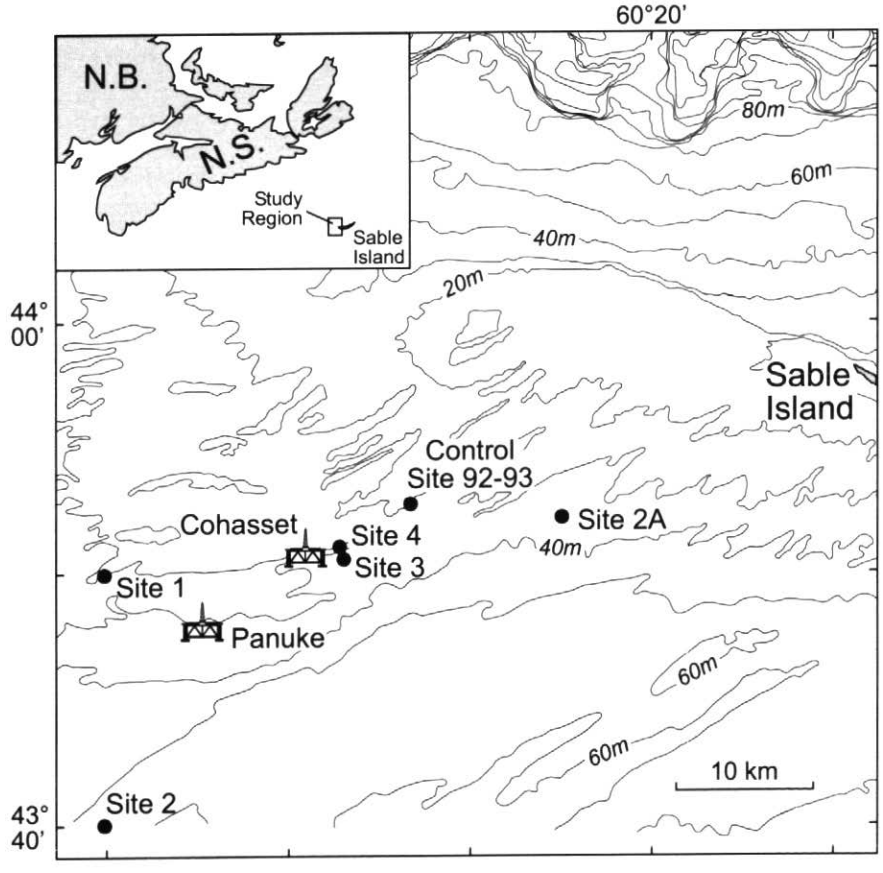

Figure 1 The location map showing the study region and instrument deployment sites on Sable Island Bank, Scotian Shelf.

Heffler, 2002) to calculate the drag-coefficient based total current shear velocity $u_{*c\text{-}CD}$. The value of $u_{*c\text{-}CD}$ thus includes no effect of wave-current interaction or sediment transport, but is due only to the sum of the grain roughness and ripple roughness, $z_{0c\text{-}GR}$. The GM86 model was then run using the grain-ripple roughness $z_{0c\text{-}GR}$ (but no roughness due to bedload transport; see next section for explanation). Therefore, the model-predicted total current shear velocity, $u_{*c\text{-}M}$, and the apparent bottom roughness, $z_{0c\text{-}M}$, were only due to the grain-ripple roughness plus the effect of wave-current interaction. Time series plots of the ratio of $u_{*c\text{-}M}/u_{*c\text{-}CD}$, $z_{0c\text{-}GR}$ and $z_{0c\text{-}M}$ are shown in Figure 3. While the total current shear velocity was enhanced 2-3 times during storms (marked as 1, 3, 5 and 8 in Fig. 2c), the enhancement was about 20% even during non-storm periods (marked as 2 and 7 in Fig. 2c). The comparison of $z_{0c\text{-}M}$ and $z_{0c\text{-}GR}$ in Figure 3b indicates that the apparent roughness $z_{0c\text{-}M}$ felt by the steady current above the wave boundary layer increased by more than one order of magnitude during storms. This roughness was enhanced 2-3 times, even during the current-dominated non-storm periods. These results clearly demonstrate that ignoring the effect of wave-current interaction will cause significant underestimates of the total current shear stress and apparent bottom roughness.

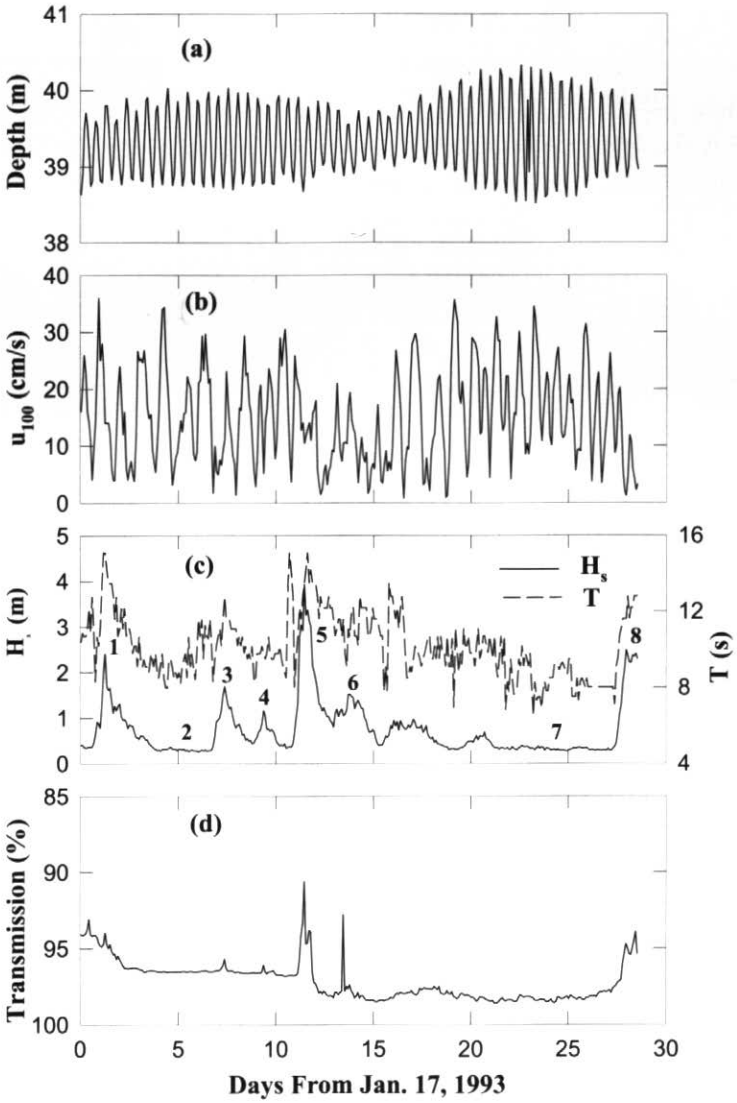

Figure 2 Time series of the RALPH data collected in the 1992-1993 winter deployment at Site 1 on Sable Island Bank: (**a**) the water depth, (**b**) mean velocity u_{100}, (**c**) significant wave height, H_s and spectral peak wave period, T, and (**d**) suspended sediment concentration 0.7 m off the seabed expressed in transmission percentage.

Thresholds of Sediment Transport Modes

Accurate prediction of sediment transport rate very much depends on the determination of threshold criteria for the various sediment transport modes, namely bedload, suspension, and sheet flow. Although these thresholds are reasonably established for waves and unidirectional flows, threshold values and field data for combined flows were largely unknown before the mid 1980s (*e.g.,* Huntley, 1986).

Nearly 700 seabed photographs were taken during the RALPH deployment at Site 1, and these photos successfully captured various seabed states, ranging from no transport, through active ripples and suspension, to sheet flows. Li *et al.* (1997) correlated these observed bed states with wave-current data to define the threshold criteria for various sediment transport modes under combined-flow conditions. Based on a modified Shields curve, Li and Amos (1995) proposed the following regression relationships for the critical Shields parameter θ_{cr} for bedload transport:

$$\log\theta_{cr} = 0.045 \qquad \sqrt{\Xi} > 3000 \tag{1a}$$

$$\log\theta_{cr} = 0.132\log\sqrt{\Xi} - 1.804 \qquad 100 \le \sqrt{\Xi} \le 3000 \tag{1b}$$

$$\log\theta_{cr} = 0.041(\log\sqrt{\Xi})^2 - 0.356\log\sqrt{\Xi} - 0.977 \qquad \sqrt{\Xi} < 100 \tag{1c}$$

where $\sqrt{\Xi}$ is the Yalin parameter defined as $[(\rho_s-\rho)gD^3/\rho\nu^2]^{0.5}$ in which g is the gravitational acceleration, D is sediment diameter, ν is the kinematic fluid viscosity, ρ and ρ_s are fluid and sediment density, respectively. For D = 0.034 cm at Site 1, eq. 1 gives $\theta_{cr} = 0.043$ which converts to a critical shear stress $\tau_{cr} = \theta_{cr}(\rho_s-\rho)gD = 2.33$ dynes/cm^2 or a critical shear velocity $u_{*cr} = (\tau_{cr}/\rho)^{0.5} = 1.51$ cm/s. The critical shear velocity for suspension, u_{*crs}, is adopted from Bagnold (1956), who believed that suspension occurs when the vertical components of the turbulent velocity are roughly equal to the grain's settling velocity, w_s:

$$u_{*crs} = 0.8w_s \tag{2}$$

For the medium sand of D = 0.034 cm at Site 1, equation 2 predicts $u_{*crs} = 3.49$

cm/s. For sheet flows, Li and Amos (1999a) have recently compiled all available sheet flow data and derived the following empirical function of the critical Shields parameter for sheet-flow θ_{up}:

$$\theta_{up} = 0.172D^{-0.376} \quad (3)$$

where sediment grain size D is in cm. For D = 0.034 cm, equation 3 gives θ_{up} = 0.61 or the critical shear velocity for sheet-flow u_{*up} = 5.8 cm/s.

In order to evaluate the applicability of these thresholds under combined-flow conditions, the time series of the skin-friction combined wave-current shear velocity u_{*cws}, obtained from the GM86 model, is plotted in Figure 4a for the Site 1 data, with various observed transport modes being represented by different symbols. The observed transition from no motion to bedload transport (rippled bed) is well defined in Figure 4a, but the boundary is clearly below the bedload critical shear velocity u_{*cr} = 1.51 cm/s. The value of u_{*cws} at the observed transition from bedload to suspension and that at the observed onset of sheet-flow transport are also substantially less than the respective threshold values for these transport modes.

Figure 4a thus shows that the enhancement of shear stress by the presence of ripples and by bedload transport is important (Li *et al.* 1997). When ripples are present, the shear stress will increase from the ripple trough to the crest. Thus, the ripple-enhanced shear velocity u_{*cwe}, not the spatially averaged shear velocity u_{*cws}, should be used to determine the onset of bedload transport. When sediment transport occurs under higher shear stresses, a portion of the flow power is spent in maintaining a thin bedload transport layer. Previous studies showed that the friction factors in these high transport stages correlate better with the thickness of the bedload layer (Wilson, 1988), and a bedload-related shear stress needs to be used for stress partitioning (Smith and McLean, 1977; Li, 1994) and transport calculation (Nielsen, 1992). Based on these results, Li *et al.* (1997) have proposed that the sum of the grain size and bedload roughnesses should be used to compute a bedload shear velocity u_{*cwb}, and it is this bedload-enhanced shear velocity that should be used to determine the onset of

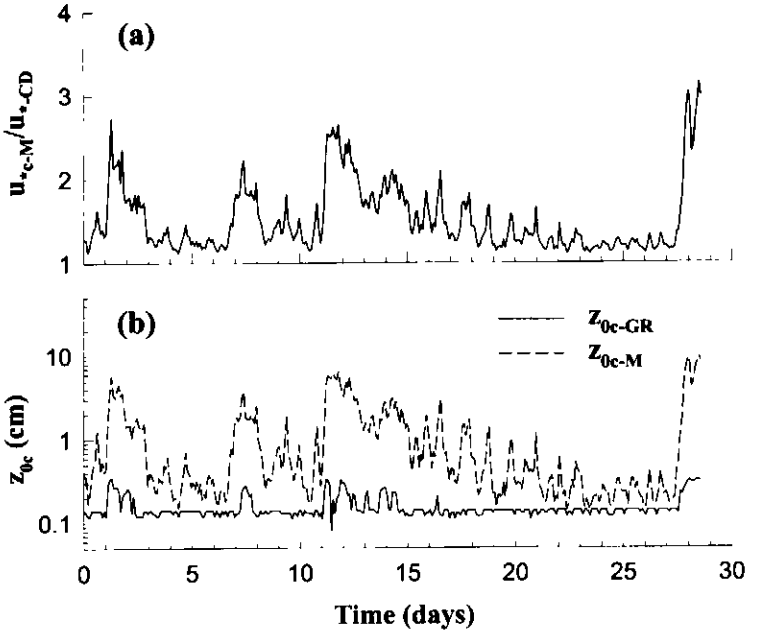

Figure 3 Time series plots of (a) the ratio of $u_{*c\text{-}M}/u_{*c\text{-}CD}$, (b) $z_{0c\text{-}GR}$ and $z_{0c\text{-}M}$ for Site 1 RALPH data to quantify the enhancement of total current shear velocity and apparent bottom roughness due to wave-current interaction.

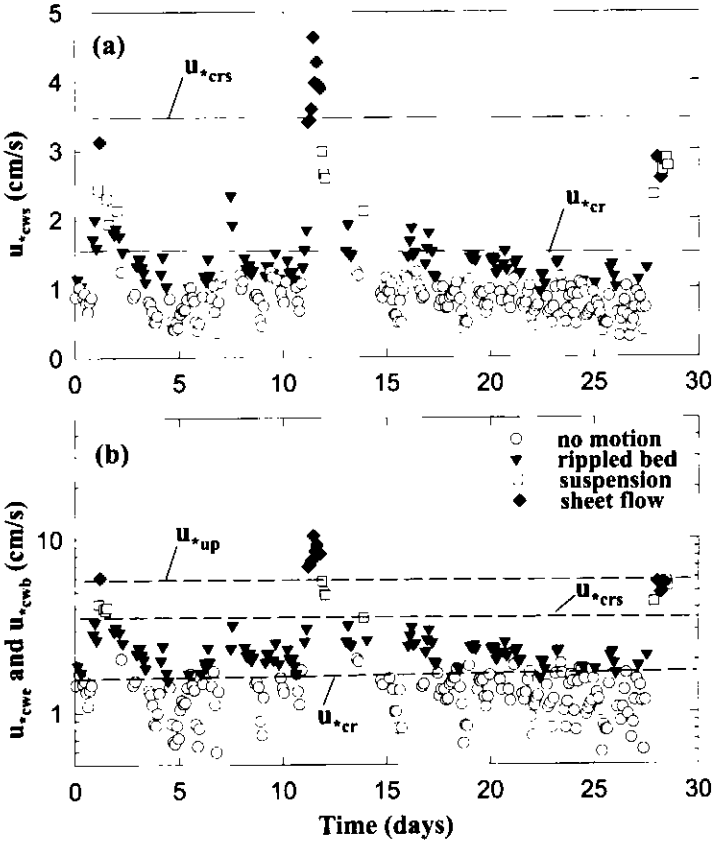

Figure 4 Time series of the combined shear velocity: (a) the skin-friction shear velocity u_{*cws} and (b) the ripple-enhanced shear velocity u_{*cwe} and bedload shear velocity u_{*cwb} for Site 1 RALPH data. Observed transport modes are indicated by different symbols. The dashed lines represent the established critical shear velocities for bedload (u_{*cr} = 1.51 cm/s), saltation/suspension (u_{*crs} = 3.49 cm/s) and sheet flow (u_{*up} = 5.8 cm/s) transport, respectively.

sand suspension and sheetflow transport under combined waves and currents. Figure 4b shows the time series plot of shear velocity for the same Site 1 data, but the ripple-enhanced shear velocity u_{*cwe} is now used for the no motion and bedload periods in which $u_{*cws} \leq u_{*cr}$, and the bedload shear velocity u_{*cwb} is used for the suspension and sheetflow periods and those bedload periods in which $u_{*cws} > u_{*cr}$. The ripple-enhanced shear velocity u_{*cwe} is calculated according to Nielsen (1986), and the bedload shear velocity u_{*cwb} is predicted from the GM86 model using the bedload roughness height algorithm derived from Sable Island Bank combined-flow field data (Li *et al.*, 1997). Figure 4b shows that the observed transitions are now in good agreement with the established critical shear velocities. Hydrodynamic data and seabed video images collected by a later deployment at a site characterized by a fine sand bed (Site 2 in Fig. 1) have supported this finding (Li and Amos, 1999b).

Partitioning Skin Friction and Form Drag Over Ripples

In shelf sediment transport, the bottom stress is conventionally obtained by measuring the velocity profile far above the sediment bed and fitting this profile to the von Karman-Prandtl equation (eq. 2 of Li and Heffler, 2002). When ripples are present, this profile-derived stress is the total current shear stress *i.e.*, the sum of the form drag and the skin friction. Since only the skin friction is responsible for sediment entrainment and transport, the incorrect use of this total stress may lead to large errors in bbl modelling and sediment transport calculations.

Based on field measurements over subaqueous dunes in the Columbia River, Smith and McLean (1977) proposed a "boundary layer within boundary layer" model to predict skin-friction shear velocity u_{*s} as well as total boundary layer shear velocity u_*. Subsequently this model has been expanded and tested by Nelson and Smith (1989) and Wiberg and Nelson (1992) against velocity measurements over fixed dunes and ripples in flume experiments. In a more focussed flume study by Li (1994), epoxy-coated hot-film sensors were used in direct measurements of velocity profiles and skin friction over mobile sand ripples of different geometries to investigate the variation of the skin-friction and form drag as a function of ripple shape and flow strength, and to test the applicability of the Smith and McLean (1977) model to mobile sand ripples. The results of this experiment indicated that the ratio of the skin friction shear velocity over the total shear velocity ranged from 0.4 to 0.7 for the experimental conditions used. For a given mean surface velocity, the average skin friction shear velocity was found to decrease with increasing ripple height and wavelength. For a given ripple geometry, the ratio of the skin friction shear velocity over the total shear velocity was not constant, but increased with the increase of flow strength. The Smith and McLean (1977) model was found to give reasonable partition of the skin friction from the total shear stress over mobile sand ripples. Semi-empirical relationships were derived that can be used to estimate the skin friction shear velocity u_{*s} from known profile-derived total shear velocity u_* and ripple geometry data.

Bedform and Bed Roughness Predictions

Accurate prediction of ripple geometry and bed roughness is crucial to the modelling of sediment transport since ripple development and bed roughness variation will directly or indirectly control the total bed stress, the near bed velocity structure, the stress partitioning, and the sediment resuspension process (Grant and Madsen, 1982; Huntley, 1986; Glenn and Grant, 1987; Cacchione and Drake, 1990; Wiberg and Nelson, 1992; Li, 1994; Vincent *et al.*, 1991 and Li *et al.*, 1996). The geometry and development of wave ripples have been relatively well studied, and several predictive models have been proposed (see Li and Amos, 1998, for references). In contrast, studies on the generation and dynamics of combined-flow ripples have been sparse (Arnott and Southard, 1990; van Rijn *et al.*, 1993). Amos *et al.* (1988) studied ripple types and stability over fine sand under nearly orthogonal waves and currents by analysing seabed photographs collected in an earlier RALPH deployment on Sable Island Bank (SIB), Scotian Shelf. Different bed types were recognized, and they were separated in plots of skin-friction wave Shields parameter (from the GM86 model) *versus* the steady-current Shields parameter (according to Sternberg, 1972). Wave-current ripples intermediate in form and orientation were not seen, however, because the deployment site was dominated by nearly orthogonal waves and currents.

Building upon this work, instrumented tripods and S4 wave-current meters were deployed at several sites in the south and southwest regions of SIB (Li *et al.*, 1997; Li and Amos, 1999b; Li *et al.*, 1999a). Using these new data as well as that of Amos *et al.* (1988), the following bed types (see Fig. 5) have been determined for combined wave and current flows:

1) *No motion.* Occurring either as bioturbated flat bed or relict ripple bed. Evidence of biodegradation is apparent and the seabed is often covered by benthos or their traces.
2) *Current ripples.* Asymmetrical in profile, sharp brink points, tabular slip faces, no crest bi-furcation, migrate in the direction of current. They can be further divided into three subtypes: *straight-crested current ripples* (C_s), with straight, continuous crests; *undulatory* (or *sinuous*) *current ripples* (C_u), with wavy, continuous crests; *linquoid current ripples* (C_l), with short, discontinuous crests curved in a tongue-like form in the downstream direction;
3) *Current dominant ripples* (C_w). Active, well-developed, asymmetrical current ripples dominate with subordinate symmetrical wave ripples present in current ripple troughs. Crests of wave ripples are discontinuous and broken by current ripple crests. Current ripples will migrate, while wave ripples are stationary.
4) *Combined wave-current ripples* (WC). Wave and current ripples with roughly equal magnitudes co-exist. Wave ripples are discontinuous and of greater sinuosity than pure wave ripples; current ripples are often triangular in plan; current ripples will migrate, while wave ripples are stationary.
5) *Wave dominant ripples* (W_c). The bed is dominated by wave ripples, but small, asymmetric, straight-crested current ripples exist in wave ripple troughs. Polygons can form due to the juncture

of the two ripple types. Wave ripples are stationary and current ripple migration is also weak.

6) *Wave ripples* (W). These ripples (and the wave dominant ripples) are generally symmetrical or slightly asymmetrical in profiles; straight, pointed crests and rounded troughs with crest bifurcations; crests are regularly spaced. Well developed, but no net migration.
7) *Saltation/suspension* (SS). Observe sand clouds or strong sediment throwing up at ripple crests. General deterioration of image clarity is evident.
8) *Large wave ripples* (LWR). Well-developed wave ripples with wavelengths greater than 40-50 cm.
9) *Upper-regime plane bed under sheet-flow* (UPB). Characterized by strong image blurring, but clearly recognized plane bed.

For combined wave-current ripples (WC), analyses of bedform video images collected over fine sand at Site 2 (Fig. 1) by Li and Amos (1999b) show that when waves and currents are co-linear, single sets of asymmetrical intermediate wave-current ripples do form. These asymmetrical intermediate wave-current ripples can be differentiated from asymmetrical current ripples by their rounded crests, straighter and more regular forms, and associated crest bifurcations. Li and Amos (1999a) also find that the large ripples observed during storms are often moulded into symmetrical, rounded and mound-like features, and these should be defined as combined-flow hummocky megaripples. LWRs and hummocky megaripples generally occur following the peaks of storms due to sediment fall out from suspension and moulding of the seabed by the long wave oscillation at this waning stage of storms.

Li and Amos (1998) propose that the ratio of the skin-friction wave shear velocity to that of the steady current, u_{*ws}/u_{*cs}, should be used to better define the various types of ripples under combined flows. Figure 6 shows the time series plot of the u_{*ws}/u_{*cs} ratio for the Site 1 RALPH data, with various types of ripples being represented by different symbols. Figure 6 demonstrates that when $u_{*ws}/u_{*cs} < 0.8$, bedforms are current or current-dominant ripples, while only wave ripples can occur if $u_{*ws}/u_{*cs} > 2$. When u_{*ws}/u_{*cs} ratio is between 1.3 and 2, bedforms will be wave-dominant ripples. Combined wave-current ripples prevail under the condition of $0.8 < u_{*ws}/u_{*cs} < 1.3$.

Among many existing wave-ripple predictors for numerical models, the more widely used ones are that of Grant and Madsen (1982) and Nielsen (1981). Both were derived using laboratory or field wave ripple data only, and several studies have shown that they are not applicable under combined waves and currents (*e.g.*, Wright, 1993; Li *et al.*, 1996; Li and Amos, 1998). The measured and model-predicted ripple height η and ripple roughness height k_{br} (Grant and Madsen, 1982; see below) are compared in Figure 7 for 35 measurements selected from the Site 1 RALPH data set. The lower panel plots the skin-friction or bedload combined shear velocity for these data. These plots indicate that both wave ripple predictors over-predict ripple height and ripple roughness height for combined waves and currents, at least for the Site 1 experimental conditions. It also shows that when $u_{*cws} < u_{*cr}$ (Fig. 7c), both methods predict no ripple formation, yet active ripples were observed in these periods. This is probably because the enhanced shear velocity caused by pre-existing ripples is higher than u_{*cr} causing the ripples to be active in this weak-transport condition.

Based on data collected on Sable Island Bank, Li and Amos (1998) have derived an explicit ripple predictor for combined waves and currents. This model separates ripples into five categories: no motion, weak-transport ripples, equilibrium ripples, break-off ripples, and upper-plane bed in sheet flow. The ripple height and steepness mainly depend on the applied shear velocity relative to critical shear velocities for bedload, ripple

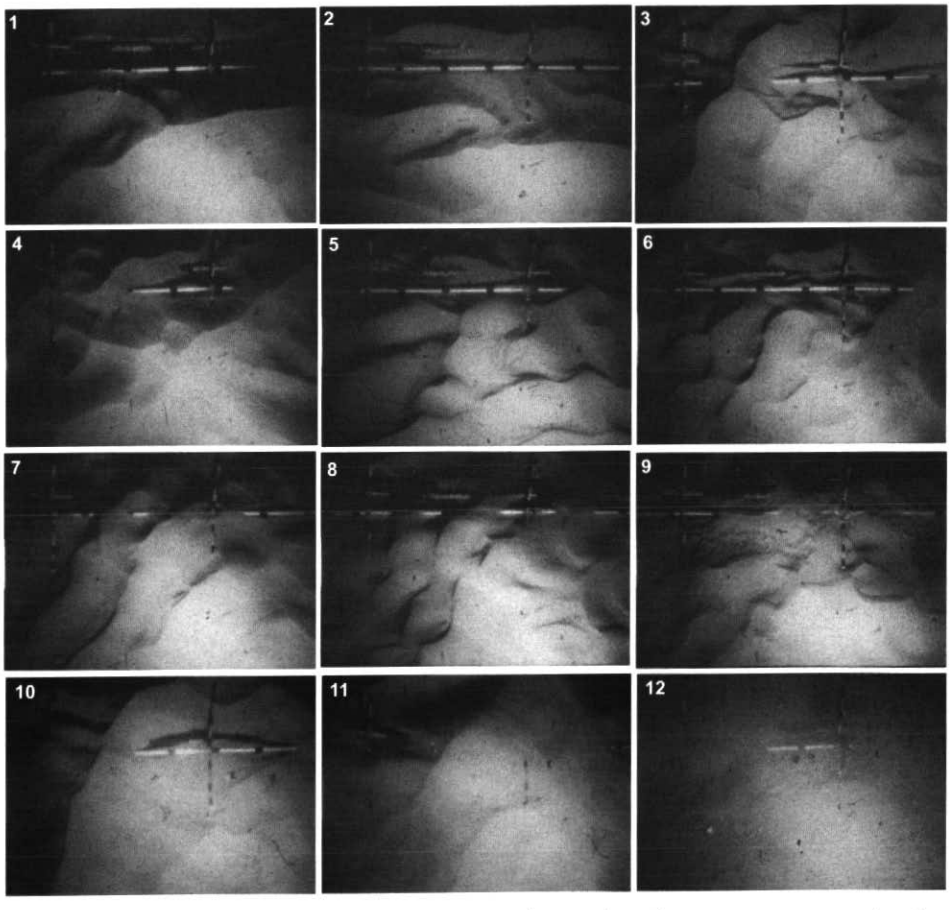

Figure 5 Images of bed types typically observed under combined waves anc currents: (**1, 2**) wave ripples; (**3**) wave-dominant ripple; (**4, 5**) combined wave-current ripples; (**6**) current-dominant ripple; (**7**) straight-crested current ripple; (**8**) linguoid current ripple; (**9**) no motion; (**10**) large wave ripple; (**11**) saltation/suspension; and (**12**) upper plane bed/sheet flow.

break-off, and sheet flow transport. For the same 35 data shown in Figure 7, this combined-flow ripple predictor has again been used to predict ripple height and ripple roughness height k_{br}. The predicted and measured η and k_{br} are compared in Figure 8. Though this is not an independent test, it shows that the proposed predictor fits well with the source data.

Bed roughness length z_0, which relates to bottom roughness height k_b by $z_0 = k_b/30$, is critical in determining the near-bed velocity profile and bed shear stress (see eqs. 2 and 4 in Li and Heffler, 2002). According to the GM86 model, the total bed roughness height k_b is the sum of the grain roughness height k_{bg}, ripple roughness height k_{br}, and bedload roughness height k_{bt}. Although k_{bg} is generally taken as 2.5D, there is a lack of consensus on the calculation of k_{br} and k_{bt}. Li and Amos (1998) have used measured ripple heights and wavelengths and various ripple roughness height algorithms in the GM86 model to predict total current shear velocity u_{*c} and apparent bed roughness length z_{0c} for selected bursts of Site 1 RALPH data. The velocity data were then used in a simplified logarithmic velocity profile method (Sternberg, 1972) to obtain profile-derived u_{*c} and z_{0c}. The comparisons of the model-predicted and profile-derived u_{*c} and z_{0c} have shown that the ripple roughness height expression $k_{br} = 27.7\eta^2/\lambda$ of Grant and Madsen (1982; λ ripple wavelength) applies well under combined waves and currents. The ripple roughness height expression $k_{br} = 8\eta^2/\lambda$ of Nielsen (1992) has also been found applicable, though it tends to under-predict for the selected data bursts (Li and Amos, 1998).

Based on laboratory flume data, various algorithms have been developed for bedload roughness height k_{bt} (*e.g.*, Grant and Madsen, 1982; Wiberg and Rubin, 1989; Nielsen, 1992). In addition to the comparison between profile-derived u_{*c} and z_{0c} and that predicted from the GM86 model using various bedload roughness algorithms (Li and Amos, 1998), Li *et al.* (1997) and Li and Amos (1999b) have also evaluated these proposed bedload roughness algorithms by comparing the bedload shear velocity u_{*cwb} predicted from the GM86 model using various k_{bt} algorithms and the established critical sheet-flow shear velocity u_{*up} for observed sheet-flow events in both Site 1 and Site 2 deployments over medium and fine sand sediments. The preliminary conclusion is that the algorithms proposed by Grant and Madsen (1982) and Wiberg and Rubin (1989) underpredict bedload roughness for combined waves and currents, and that the expression of Nieslen (1992) and a new algorithm proposed by Li *et al.* (1997) based on recent SIB data give reasonable predictions under combined-flow conditions.

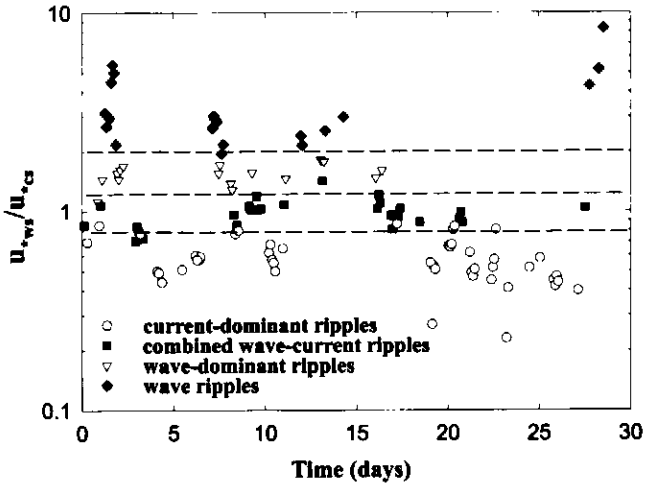

Figure 6 The time series plot of skin-friction wave shear velocity to skin-friction current shear velocity u_{*ws}/u_{*cs} for selected bursts of Site 1 Ralph data. Observed ripple types are indicated by different symbols.

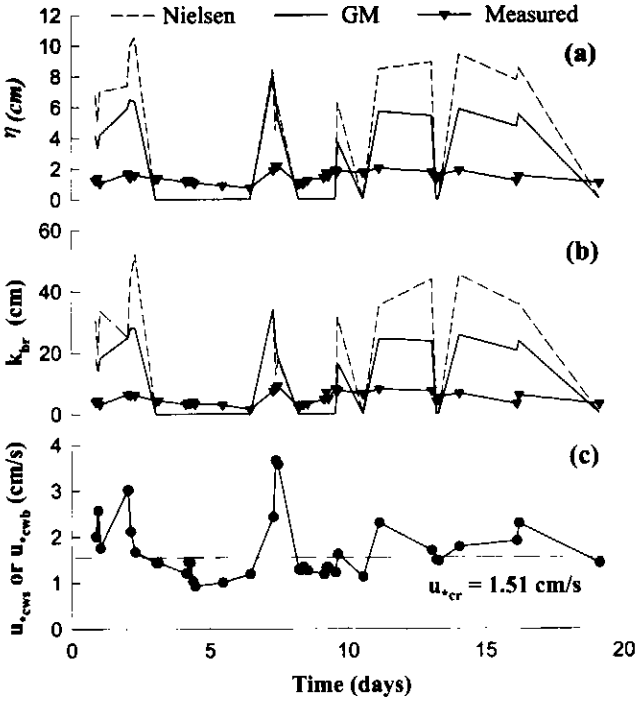

Figure 7 The time series of (a) the measured and model-predicted ripple height η, (b) the measured and model-predicted ripple roughness height k_{br} and (c) the skin-friction or bedload combined shear velocity for selected bursts from Site 1 Ralph data. The dashed and solid lines in (a) and (b) respectively represents the predictions by the Nielsen (1981) and Grant and Madsen (1982) models. The dashed line in (c) is the threshold shear velocity for bedload transport.

Sediment Transport Rate Prediction

Sediment Transport Model Calibration

Because of the extensive research on sediment transport under unidirectional flow, sediment transport rate predictions on continental shelves have primarily relied on formulae derived for rivers or channel flows. The complex non-linear relationships between waves, currents, and seabed, however, have made it extremely difficult to test the applicability of these formulae in marine environments. Limited sand tracer experiments in marine environments showed 2 orders of difference between measured and predicted transport rates (*e.g.*, Heathershaw, 1981). Earlier reviews have found that there was no consensus on which formulae worked the best on continental shelves, and the paucity of field data severely limited our ability to calibrate sediment transport models (Huntley, 1986; Bowen, 1986).

One of the main objectives of the GSC's Sable project has been to collect high-quality field data for the calibration of sediment transport models. Ripple height, migration rates, and concurrent hydrodynamic data collected using RALPH at several sites on Sable Island Bank have been used to calibrate the GSC sediment transport model SEDTRANS (Li and Amos, 1995; Li *et al.*, 1997; Li and Amos, 2001). For bedload transport rate, the ripple height η and migration rate R_m can be used to derive the mean mass transport rate per unit width per unit time from:

$$Q_m = 0.5\rho_b \eta R_m \qquad (4)$$

where ρ_b is the bulk sediment density. The measured ripple heights and migration rates of the 1993 Site 1 RALPH data over medium sand and the 1982 RALPH data over fine sand have been used to obtain the measured bedload sediment transport rates Q_m. The wave and current data are then used in SEDTRANS to predict sediment transport rate. Figure 9 plots the time series of the measured sediment transport rate for 1993 Site 1 data in comparison with that predicted by SEDTRANS using the Einstein-Brown (Brown, 1950) bedload formula and the skin-friction shear stress τ_{cws}. These plots show that the use of the skin-friction shear stress (Fig. 9b) under-predicts the frequency and magnitude of sediment transport under Site 1 field conditions. This under-prediction is most likely due to neglecting the shear stress enhancement by ripples discussed earlier. Using the ripple-enhanced shear stress τ_{cwe} gives better prediction of the frequency of sediment transport (Fig. 9c), although the magnitude seems to be over predicted. To further evaluate the suitability of the average skin-friction shear stress and the maximum ripple-enhanced shear stress in predicting sediment transport rate, τ_{cwe} was first used to determine the onset of sediment transport. τ_{cws} and τ_{cwe}, respec-

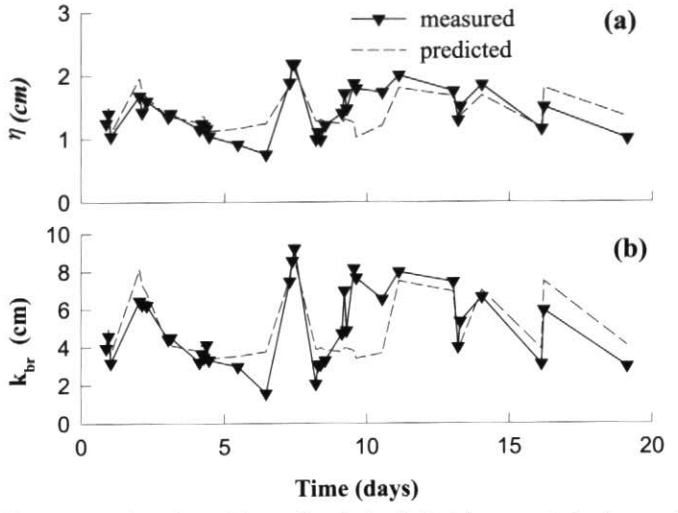

Figure 8 The measured and model predicted ripple height η and ripple roughness height k_{br} using the proposed combined-flow ripple predictor.

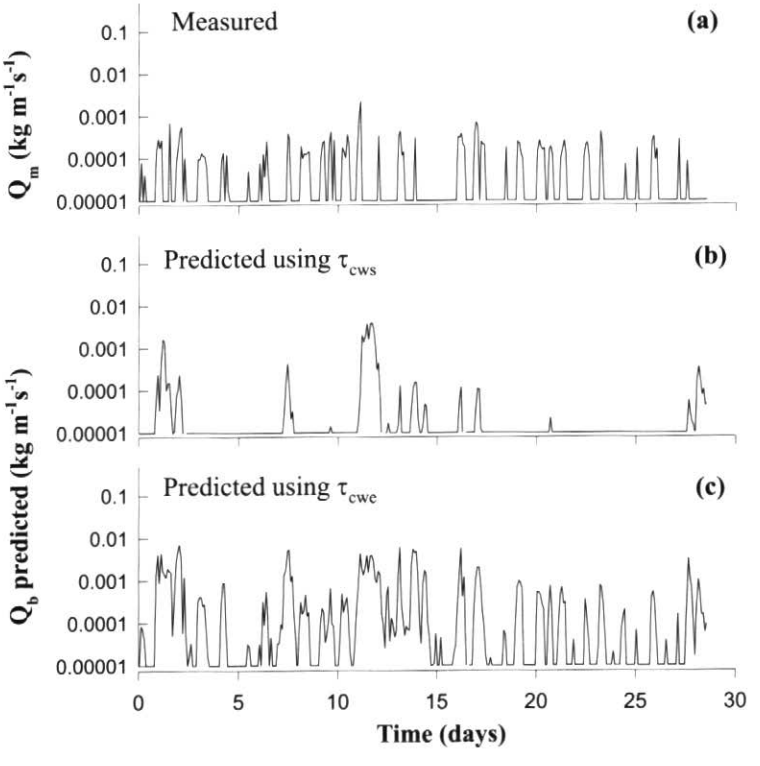

Figure 9 Time-series plot of (**a**) the measured sediment transport rate Q_m in comparison with the predicted sediment transport rates, Q_b, by the Einstein-Brown formula using (**b**) the spatially averaged skin-friction shear stress τ_{cws}, and (**c**) the ripple-enhanced shear stress, τ_{cwe}.

tively, were then used in SEDTRANS to obtain the predicted Einstein-Brown bedload transport rates. The measured and predicted sediment transport rates are compared in Figure 10. These data show that sediment transport rates can be under predicted by a factor of 5 when the average skin-friction shear stresses are used (Fig. 10a). In contrast, the use of the ripple-enhanced shear stresses results in an over prediction by up to a factor of 5 at higher transport rates (Fig. 10b).

Li and Amos (2001) believe that this difference is due to the variation of shear stress over ripples. When ripples are present, bed shear stress increases from ripple trough to crest (*e.g.,* Wiberg and Nelson, 1992; Li, 1994). Thus, predictions using the maximum enhanced shear stress at the ripple crest τ_{cwe} will give the highest transport rate across the ripple wavelength and will not be representative of the mean transport rate averaged across the ripple wavelength. Since sediment transport rate is proportional to the third or higher power of shear velocity, the mean transport rate averaged over the ripple wavelength will be skewed toward the higher values, causing the under prediction when using the spatially averaged skin-friction shear stress τ_{cws}. Therefore, an effective shear stress between these two values needs to be found for better prediction of the sediment transport rate.

Based on the facts that the ripple-enhancement of shear stress is most effective for ripples in the weak-transport and equilibrium ranges (in which ripple steepness is at the maximum) and that the effective shear stress should asymptotically approach the average skin-friction shear stress at higher transport stages when the ripple steepness approaches zero, Li and Amos (2001) proposed the scheme of the effective shear stress τ'_{cws} as a function of bedform development stages (see eq. 5a, b, c in box below),

$$\tau'_{cws} = (\tau_{cr} + \tau_{cwe})/2 \qquad u_{*cwe} \geq u_{*cr} \text{ and } u_{*cwb} < u_{*bf} \qquad (5a)$$

$$\tau'_{cws} = [1/(2+\sigma)](\sigma\tau_{cr} + \tau_{cws} + \tau_{cwe}) \qquad u_{*bf} \leq u_{*cwb} < u_{*up} \qquad (5b)$$

$$\tau'_{cws} = \tau_{cws} \qquad u_{*cwb} \geq u_{*up} \qquad (5c)$$

where $\sigma = (u_{*up} - u_{*cwb})/(u_{*up} - u_{*bf})$ is a ripple break-off parameter. The physical meaning of equation 5 is that in the weak-transport and equilibrium ranges (5a), sediment transport occurs on only a portion of the ripple stoss slope over which the bed shear stress increases from τ_{cr} to τ_{cwe}. The average of these two values is taken to be the effective bed shear stress at these stages. In the ripple break-off range (5b), all three shear stresses (the critical, the average, and the ripple-enhanced) are important, with the effect of τ_{cr} diminishing as transport approaches sheet-flow mode. Finally when upper-plane bed is reached (5c), there will be no ripple enhancement and the effective shear stress is now equal to the average bed shear stress.

The effective shear stresses given by equation 5 were used in SEDTRANS to predict sediment transport rates from four popular formulae: the Engelund and Hansen (1967) total load equation, the Einstein-Brown (Brown, 1950) bedload equation, the Bagnold (1963) total load equation, and the Yalin (1963) bedload equation. The predicted and measured sediment transport rates are compared in Figure 11. Compared to Figure 10, these plots show that using the effective shear stresses given by equation 5 reasonably predicts sediment transport rates for both fine and medium sand and that the error is generally less than a factor of 5. A large portion of this error is probably due to the uncertainty in the field measurements of ripple height and ripple migration rate. Figure 11 also shows that the Einstein-Brown bedload method and the Bagnold total load method give the best prediction of sediment transport rates under combined-flow conditions. Larger scatter exists in the prediction by the Engelund-Hansen total load method, while the Yalin method tends to under predict sediment transport rates at the low transport stages and slightly over predict at higher transport stages.

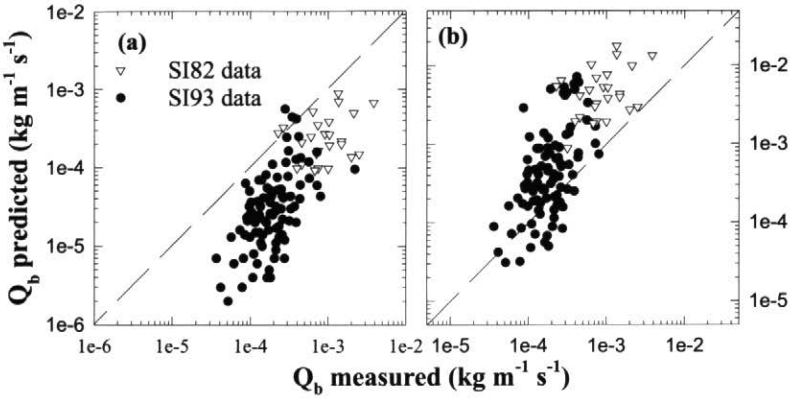

Figure 10 Scatter plots of the measured and predicted sediment transport rates from the Einstein-Brown formula using (**a**) the spatially averaged skin-friction shear stress and (**b**) the ripple-enhanced shear stress. Circles are data from the 1993 Site 1 deployment over medium sand, and triangles are data from the 1982 deployment over fine sand. The dashed lines represent perfect agreement.

Sand Resuspension and Reference Concentration C_0

Rouse (1937) type equations (eq. 6, Li and Heffler, 2002) are widely used to predict suspended sediment concentration (ssc) profiles. However, our limited understanding of sand resuspension processes renders significant errors in the application of this type of equation. Besides the lack of good-quality field data, other factors that hinder our ability to accurately predict ssc on shelves include the uncertainty in understanding the sand resuspension mechanism and hence the calculation of the reference concentration C_0 (eq. 6, Li and Heffler, 2002), vertical sorting of grain size and hence settling velocity w_s of the suspended sediment, and the bed armouring and proper selection of τ_{cr} in heterogeneous sediment (*e.g.,* Huntley, 1986; Cacchione and Drake, 1990; Nittrouer and Wright, 1994).

The value of C_0 mainly depends

on the empirical resuspension co-efficient γ_0 and the excess shear stress, which is the difference between bottom shear stress τ_{cws} and the critical shear stress for bedload transport τ_{cr}. As τ_{cws} can be reasonably predicted by combined-flow boundary layer models and τ_{cr} can be well defined for reasonably well-sorted, non-cohesive sediment, the main problem therefore lies with the determination of the resuspension coefficient γ_0. Earlier researchers assumed γ_0 to be constant (*e.g.*, Smith and McLean, 1977). Subsequent studies have found a wide range of γ_0 values (Wiberg and Smith, 1983; Kachel and Smith, 1986; Hill *et al.*, 1988) and that γ_0 decreases with the increase of bed shear stress (Drake and Cacchione, 1989; Vincent *et al.*, 1991). Although bed armouring and compaction (for silt and mud deposits) have been suggested as causes of the variation of γ_0 (*e.g.*, Cacchione and Drake, 1990), a more obvious factor is the effect of bedform development on sand resuspension. Using simultaneously measured wave, current, and near-bed ssc data, Vincent *et al.* (1991) and Li *et al.* (1996) have shown that γ_0 over a sand bed decreases systematically with the increase of bed shear stress. Li *et al.* (1996) further demonstrated that the decrease of ripple roughness and hence the reduction of vortex activity over break-off ripples are the causes of the decrease of γ_0 with the increasing shear stress. Figure 12 shows the scatter plot of $\log\gamma_0$ *versus* the logarithm of the normalized excess shear stress, $\log\tau_*$, for the data from both Vincent *et al.* (1991) and Li *et al.* (1996). It clearly shows that in the ripple break-off range, $\log\gamma_0$ decreases from 10^{-3} over low-transport ripple bed to 10^{-4} over high-transport plane bed as $\log\tau_*$ increases from 0.2 to 1.2. In the equilibrium range ($\log\tau_* < 0$), the limited data seem to indicate a trend of increasing γ_0 with bed shear stress. Comparison between the measured and predicted ssc showed that using a time-variable γ_0 in the modified Rouse equation significantly improved the prediction of ssc profiles under combined waves and currents (Li *et al.*, 1996).

Morphodynamics of Sand Ridges on Sable Island Bank

The NE-SW trending sand ridges on Sable Island Bank are one of the most striking morphological features on the Scotian Shelf. Their morphology, migration, and interaction with wave-current dynamics is not only one of the most important engineering issues for offshore energy development, but also a critical component of the regional sediment transport pattern on SIB.

Following the earlier classification and descriptive work of Amos and King (1984), there have been several recent studies that focus on the morphology and stability of the sand ridges on SIB. Hoogendoorn and Dalrymple (1986) and Dalrymple and Hoogendoorn (1997) analyzed seismic/sidescan data, Canadian Hydrographic Service (CHS) bathymetric data, as well as vibrocores and grab samples to understand the morphology, migration, and internal structures of these sand ridges. They separated the sand ridges into two orders: first order ridges with average height and wavelength (spacing) of 12 m and 6.4 km, respectively, and second order ridges with average height and wavelength of 5 m and 1.5 km. The scale of ridges decreases from west to east, the maximum ridge height decreasing from 20 m in the west to 3.2 m in the east. Most ridges show asymmetric profiles, with steeper eastern (lee) flanks. There is a general trend of decreasing grain size from ridge trough to crest: coarse and very coarse gravelly/shelly sands on the lower western flank progressively changing to fine sand over the ridge crest and over most of the eastern flank. Smaller bedforms, *i.e.*, very-large dunes (sand waves) and small to large dunes (megaripples), are found superimposed on sand ridges in the west and central parts of the ridge field. These authors believe that strong obliquely onshore, storm-driven flows cause the eastward migration of the sand ridges at rates as high as 50 m/year. On the contrary, Ingersoll and Ryan (1997) have compared repetitive multibeam surveys and 1982 CHS bathymetric data charts of SIB and found negligible to very low migration rates of the sand ridges on the bank. This conclusion, however, is only tentative because of the large navigation error and low density of the CHS data.

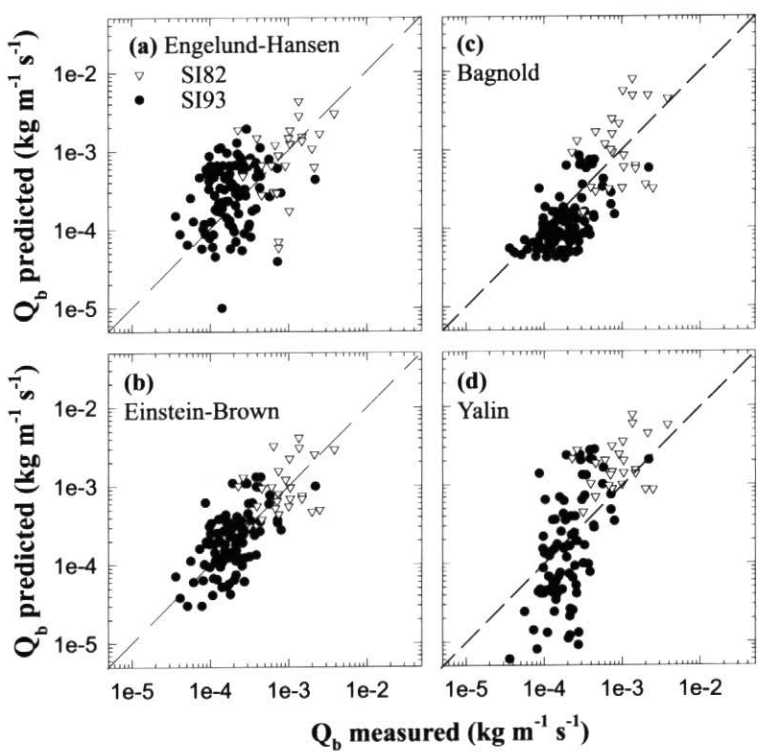

Figure 11 Scatter plots of the measured and predicted sediment transport rates using the proposed effective shear stress: (**a**) the Engelund-Hansen total-load equation, (**b**) the Einstein-Brown bedload equation, (**c**) the Bagnold total-load equation and (**d**) the Yalin bedload equation. Circles are data from the 1993 Site 1 deployment over medium sand, and triangles are data from the 1982 deployment over fine sand. The dashed lines represent perfect agreement.

In order to obtain better understanding of the morphology and dynamics of the sand ridges, GSCA has conducted repetitive multibeam bathymetry surveys of the sand ridges at selected sites on SIB since 1996 (Li *et al.*, 1999b). Figure 13 shows the shaded relief mosaic of an area to the west-southwest of Sable Island. The seabed is dominated by the NE-SW trending sand ridges, which show an average height of 4.5 m and spacing of 1.2 km. The profiles of the ridges are symmetrical to slightly asymmetrical. The steeper sides of the asymmetrical ridges can face to either the east or the west. Very large dunes (sand waves) are superimposed on the sand ridges. The crests of these dunes are generally NNE to SSW at 20°- 30° to the ridge crest lines. The average height and spacing of the dunes are variable, but are generally around 0.6-0.8 m and 80-220 m, respectively. Repetitive surveys spanning 5 years will be processed and compared to quantify the migration rate and direction of the sand ridges and associated dunes. Efforts have also begun to collect sidescan and seismic data, vibrocores, grab samples, and *in situ* sediment transport data using RALPH and S4 current meters along transects across sand ridges at selected sites on SIB. These data will be combined with the repetitive multibeam surveys to improve our knowledge of the morphology and migration of these sand ridges and of the transport mechanisms that control the migration process.

Application of Sediment Transport Models

As one-dimensional physical sediment transport models have been continuously upgraded and, to some extent, calibrated with field data, some attempts have been made to apply these models to predict regional sediment transport patterns. Amos and Judge (1991) applied the GSC sediment transport model SEDTRANS to predict sediment transport patterns on the Grand Banks and the Scotian Shelf for storms of different return intervals. The Engelund and Hansen (1967) total load formula and a single grain size of 0.35 mm were used in running SEDTRANS.

The Grand Banks

Storms of 32, 10 and 1 year return intervals were used for the Grand Banks. As expected, the predicted sediment transport rates decreased substantially with the reduction of storm intensity. Transport of sediment was predicted over the majority of the Banks for the 1:32 year storm (Fig. 14). The maximum transport rate was up to 0.1 kg $m^{-1}s^{-1}$ and occurred in the shallow water over the central and southeastern Grand Banks. The general pattern of sediment transport showed a southward and southeastward motion on the northern Banks, eastward on the northwestern Banks, and to the east and southeast on the central, eastern and southern Banks. An exception is the southwestward transport over a small area on the southeastern Banks that causes sediment convergence immediately to the west of Southeast Shoal (Fig. 14).

For the 1:10 year storm, the strongest sediment transport occurred on the northwestern Banks and was up to 1 kg $m^{-1}s^{-1}$. Transport rates over the remainder of the Banks, however, were

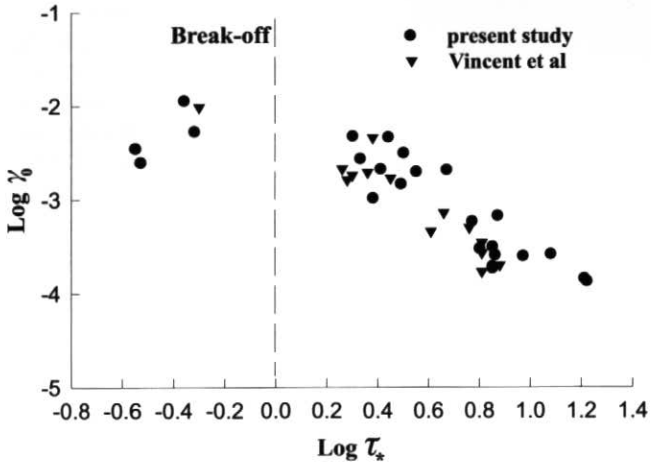

Figure 12 Variation of sand resuspension coefficient γ_0 with the normalized excess shear stress τ_*: circles representing data from this study and triangles data of Vincent *et al.* (1991). The vertical dashed line indicates ripple breakoff condition.

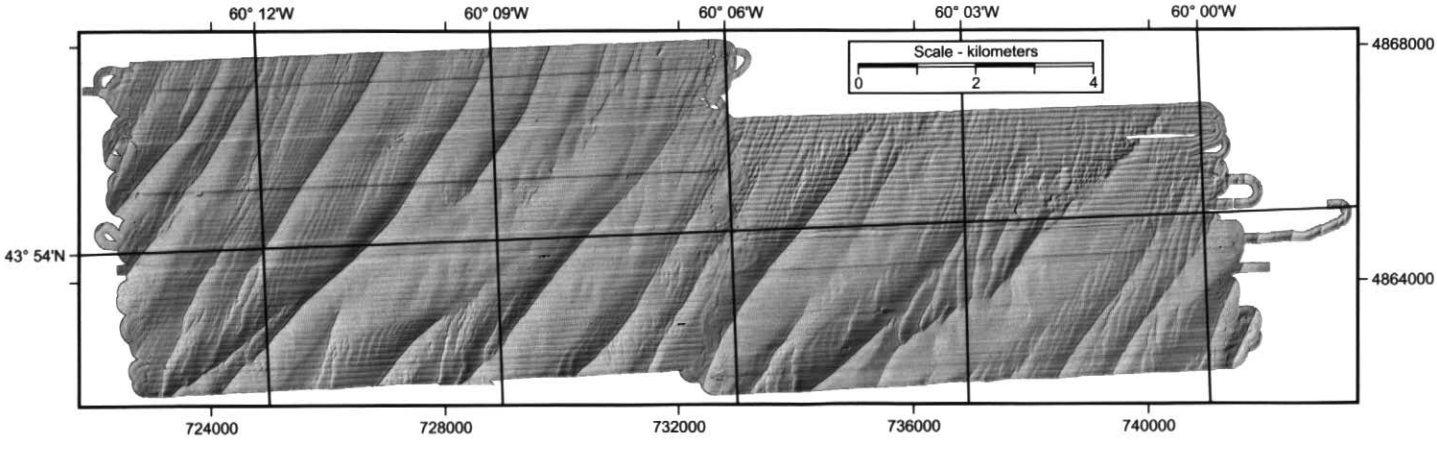

Figure 13 The shaded relief multibeam mosaics of an area to the west-southwest of Sable Island.

generally 1 order magnitude lower than that of the 1:32 year storm. The predicted sediment transport pattern was very similar to the 1:32 year storm with one exception: sediment transport was to the south and southeast over the entire southern Banks. Thus, the sediment convergence on the southeastern Banks predicted for the 1:32 year storm did not occur for the 1:10 year storm.

For typical annual (1:1 year) winter storms, the predicted sediment transport rates were considerably lower over much of the region. The highest rate of $5x10^{-2}$ kg $m^{-1}s^{-1}$ was again over the northwestern Banks. No appreciable transport was predicted on the northern Banks and in areas deeper than 100 m. The sediment transport pattern was similar to those of the other storms in the northern and western Banks, but differed over the southern part and over the tail of the Banks: sediment transport was westward and southwestward on the southern and southeastern Banks.

The Scotian Shelf and Gulf of Maine

The 1:4 year storm was used to model sediment transport for the Scotian Shelf-Gulf of Maine region. The results indicated that sediment transport on the Scotian Shelf was also storm dominated, but significantly modulated by the fluctuation of tidal currents. During the peak of the 1:4 year storm, the transport rate of 0.35 mm sand at Venture (east of Sable Island in about 20 m depth) reached 10^{-2} kg $m^{-1}s^{-1}$ under peak tidal flow and decreased to10^{-4} kg $m^{-1}s^{-1}$ under slack tides. Figure 15a shows the model-predicted sediment transport pattern when the storm peak coincided with the peak ebb tidal flow. Highest transport rates occurred on Georges Bank and Sable Island Bank, reaching 1.0 and 0.1 kg $m^{-1}s^{-1}$, respectively. Sediment transport direction was to the east and southeast on Georges Bank, western Scotian Shelf, and southern Sable Island Bank (SIB), and to the northeast on northern SIB and Banquereau. When the peak flood tidal flow coincided with the peak of the storm (Fig. 15b), predicted transport rates were reduced over most of the region and were negligible on Banquereau. The maximum transport rate on Georges Bank was around 0.5 kg $m^{-1}s^{-1}$ and that on Sable Island Bank decreased to 0.05 kg $m^{-1}s^{-1}$. Predicted transport on Georges Bank, in Northeast Channel, and on western Scotian Shelf was generally northward, aligned with the northerly tidal flow into the Bay of Fundy. Transport direction on Sable Island Bank was generally to the northeast.

In general, sand transport on the banks on Scotian Shelf is to the east and northeast, and this results from the combined effects of wind-driven currents and waves during winter storms. Exceptions are Georges Banks, Northeast Channel, and the bars around Sable Island where sediment transport is dominated by tidal currents. The decrease of the sediment transport rate at the northern margin of SIB and the sediment accretion in the vicinity of Sable Island were predicted by the model. These patterns support the concept of an "hydraulic fence" to shelf-edge sand ridge development and the absence of sand "spill-over" to adjacent basins.

Using the recently upgraded and calibrated SEDTRANS92 (Li and Amos, 1995), Anderson (1995) ran the 2-D, time-dependent model SED94 to predict the sediment transport pattern on SIB for the so-called "storm of the century" event (1:100 year storm in which peak significant wave height reached 16 m). When the peak of this intense storm coincided with the peak of the flood tidal flow, strong sediment transport was predicted over the entire Sable Island Bank. The highest transport rates were up to 2.7 kg $m^{-1}s^{-1}$ and occurred to the west of Sable Island. Sediment transport direction was to the north and northeast on the western and northern Bank, and generally to the east and southeast on the southern and eastern parts of the Bank. Similar transport rates were also predicted when the storm peak coincided with the peak of the ebb tidal flow, with the maximum rates of about 2.7 kg $m^{-1}s^{-1}$ occurring to both the west and east of the Sable Island. The sediment transport direction, however, was now predominantly to the south and southeast on the entire Bank.

Queen Charlotte Island Shelf

Amos *et al.* (1995) have applied SEDTRANS to predict the storm-enhanced sand transport on the inner Queen Charlotte Island shelf, western Canada, and used this to interpret beach erosion and sand bar formation in this area. The model predictions showed that the tidally induced sediment transport was to the northwest, and restricted to the shallow waters over the northern end of a sand bank (Fig. 16a). The maximum rate was about $5x10^{-4}$ kg $m^{-1}s^{-1}$. During a 1:5 year storm, however, sediment transport was two orders of magnitude higher, reaching $5x10^{-2}$ kg $m^{-1}s^{-1}$ and was predicted over

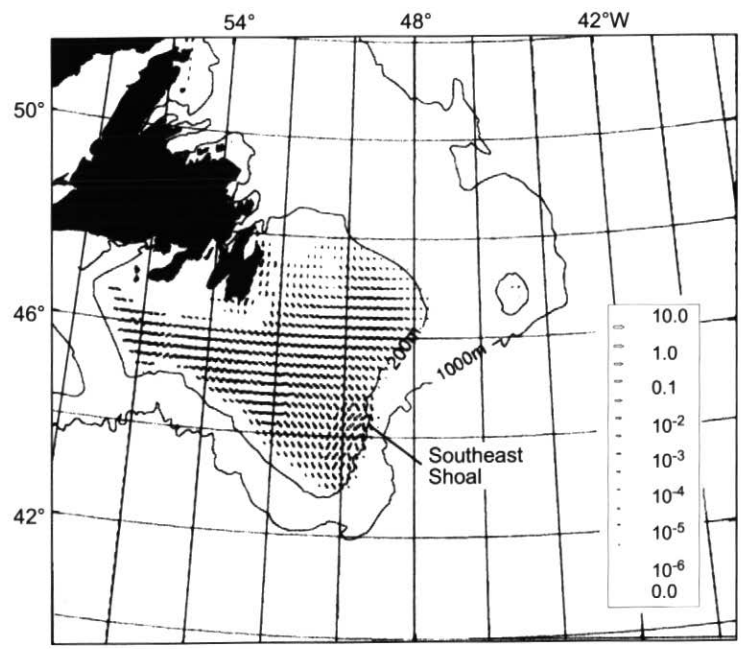

Figure 14 Regional sediment transport pattern predicted for the Grand Banks assuming D = 0.35 mm and 1:32 year storm. The arrows indicate sediment transport rate in kg m^{-1} s^{-1}.

the entire region (Fig. 16b). The strong sediment transport during the storm was largely northward alongshore and was suggested to be the cause of the continued erosion of the beach on the eastern shore of the Island. The decrease of sediment transport rates from south to north was believed to cause the sediment accretion and sand bar formation at the northern end of the region.

PROJECTED FUTURE RESEARCH PRIORITIES

The results of modelling, field measurements, and surveys, both internationally and in Canada, have clearly demonstrated that storm-generated waves, wind-driven flows, tidal currents and intruding oceanic circulation are all capable of producing strong bed shear stresses and causing episodic sediment transport on most continental shelves of the world. Over sandy shelves, this transport is manifested as occurrence of a variety of active or intermittently active bedforms ranging from small ripples to gigantic sand ridges. In addition, sediment transport on continental shelves nearly always occurs as the result of the combined effects of surface waves and steady currents. Any measurement programs or modelling efforts that neglect the interaction between waves and currents will inevitably underestimate the bed shear stresses and sediment transport rates.

Major advances have been made in the last 10-15 years in field instrumentation and combined-flow bottom boundary layer theory. The application of advanced sensors and instruments in field measurement programs has, in turn, led to significant improvement in our understanding of bbl dynamics and sediment transport processes on shelves, *e.g.,* the enhancement of shear stress and bottom roughness due to wave-current interaction, the explicit sediment transport thresholds and ripple predictors for combined waves and currents, partly calibrated sediment transport models, effects of bedform development on sand resuspension, and the characteristics and distribution of sand ridges on outer shelf sand banks. However, we are still far from a comprehensive understanding of bbl dynamics and sediment transport processes. Reviews by this and other articles (Wright, 1989; Cacchione and Drake, 1990; Nittrouer and Wright, 1994) have identified several aspects that require significantly more research:

1) *Fuller tests of the combined-flow bottom boundary layer theories.* The development and application of combined-flow bbl models (*e.g.,* Grant and Madsen, 1986) is a major advance in shelf sediment transport studies. Estimates of total current shear velocity and apparent roughness length using velocity profiles measured above the wave boundary layer have verified certain aspects of these models. However, the experiments to date have been either conducted over mud-rich sediments that do not produce well-formed bedforms, or the physical bed roughness and its temporal variation were not well specified. Therefore high-quality field data of wave-current dynamics and seabed roughness in diverse shelf and nearshore environments are still required to test the applicability of this type of model over a wide range of grain size and bed roughness. More critically, measurements of flow dynamics and skin-friction shear stress within the thin wave-current boundary layer on continental shelves hardly exist. Therefore, the prediction of the skin-friction shear stress by the model remains untested. Sensors for this kind of measurements are not yet available, although laser velocimetry and Acous-

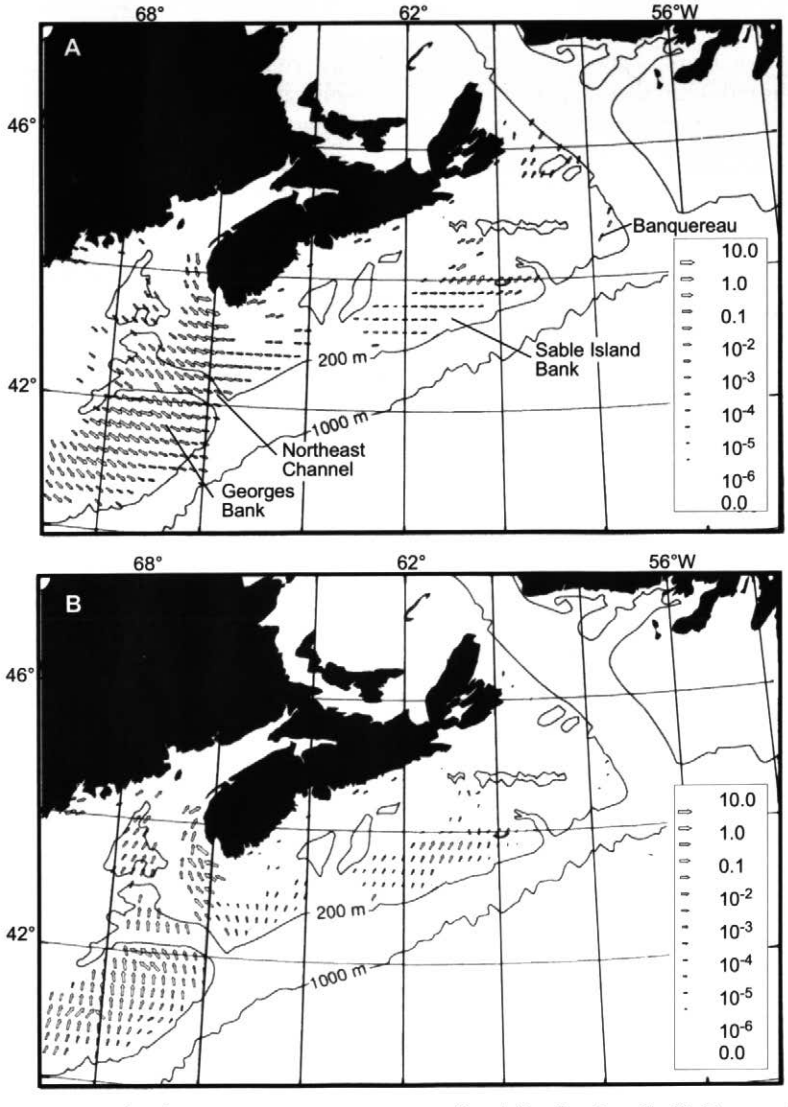

Figure 15 Regional sediment transport pattern predicted for Scotian Shelf–Georges Bank area assuming D = 0.35 mm and 1:4 year storm with storm peak coinciding with (**a**) the peak ebb tidal flow and (**b**) peak flood tidal flow. The arrows indicate sediment transport rate in kg m^{-1} s^{-1}.

tic Doppler Current Profiler (ADCP) techniques can potentially be further developed for this type of close-to-bed measurements.

2) *The extension and fuller test of the proposed sediment transport thresholds and ripple predictor for combined-flow conditions.* The recently proposed combined-flow sediment transport thresholds and ripple predictor (Li *et al.*, 1997; Li and Amos, 1998 and 1999b) were based on limited field data over medium sand and, to a lesser degree, over fine sand. More field data are needed so that these can be extended and fully tested over a wider range of sediment grain size and wave-current conditions.
3) *Derivation and calibration of a model for the prediction of suspended sediment concentration and grain size profiles on continental shelves, focussing on the effects of bedforms and bed armouring on sand resuspension.* Suspension transport is often the dominant mode of transport on many continental shelves. Although significant effort has been made in the past, our understanding of sediment resuspension processes and ability to predict suspended load transport are at best preliminary. The optical and acoustical techniques typically used for suspension measurements cannot discriminate the effects caused by concentration change from that due to particle size variation. Bedform development is also known to have great effect on the resuspension processes. Furthermore, the response of a natural sediment of mixed grain sizes to an applied shear stress can be quite different from that of uniform sediment because of such factors as grain shielding, selective entrainment and transport, and armouring of the bed by coarse size fractions. Theories and models are thus greatly needed that will incorporate the effects of bedform development and bed armouring in the prediction of sand resuspension and suspended sediment concentration profiles. The multi-frequency Acoustic Backscatter Sensor (ABS) techniques (*e.g.*, Hay and Sheng, 1992) should be combined with pump sampling to measure both concentration and particle size profiles for the derivation and calibration of the models. Given the complexity of the processes and multiple factors involved, the models should be derived and tested first in laboratory experiments and then extended to field programs.
4) *Further development and calibration of sediment transport models.* As our understanding of the bbl dynamics and sediment transport processes advances, these results need to be continually incorporated into sediment transport models. Algorithms need to be developed and included in the models so that changes of bedforms, grain size distribution of bottom sediment, and the concentration and particle sizes of suspended sediment are updated for each time step and passed on to the next time step. Due to the lack of viable techniques for direct bedload measurements, accurate information of bedform geometry and migration rates (probably using the rotary sidescan sonar techniques) should be combined with simultaneous measurements of waves, currents, and sediment suspension to provide full calibration of sediment transport models for the prediction of total load transport. Accurate estimates of suspended load transport should be

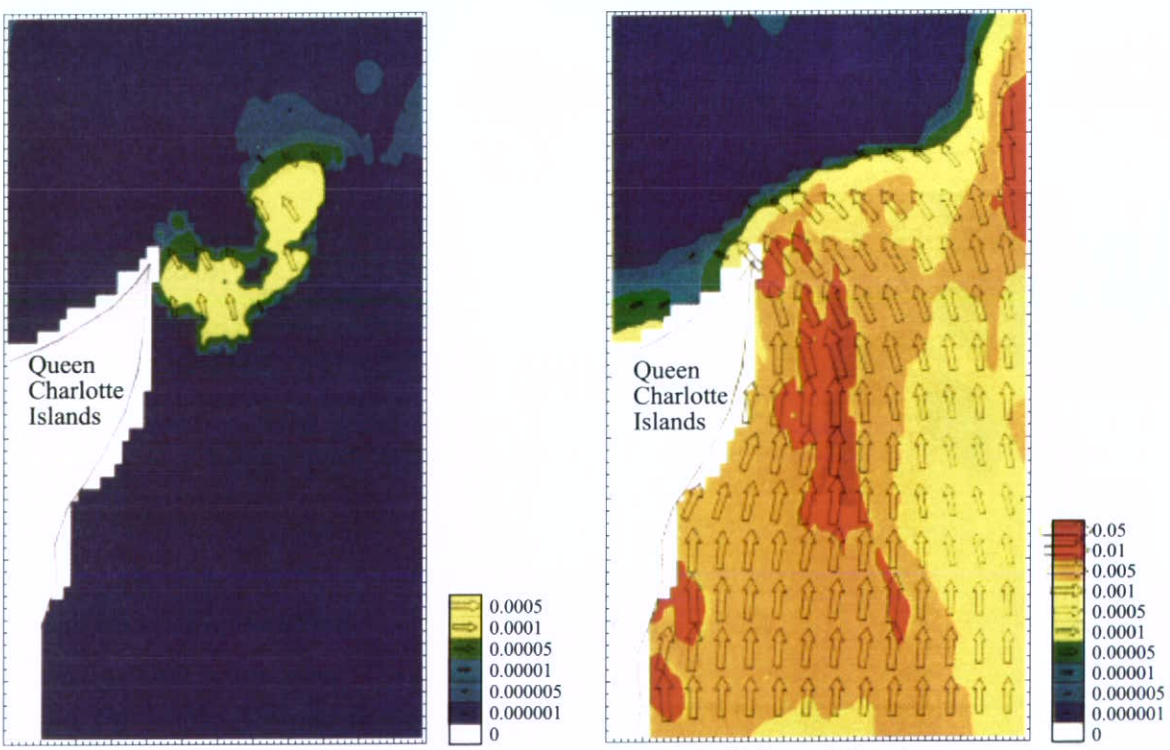

Figure 16 Regional sediment transport pattern predicted for the inner Queen Charlotte Islands Shelf using field grain size data and 1:5 year storm: (**a**) tidal current only and (**b**) storm-enhanced transport. The arrows again indicate sediment transport rate in kg m^{-1} s^{-1}.

obtained from the integration of high-resolution velocity and suspension profiles measured by the combined ABS and ADCP technologies. As for 2-D models, limited predictions of regional sediment transport on the Scotian Shelf suggest the need for a major, multi-institutional field program. Instrument packages should be deployed at several strategically selected sites to obtain simultaneous measurements of waves, currents, bedforms, and sediment transport. These data will be used to refine and/or calibrate regional wave propagation, current circulation and sediment transport models for an entire shelf region. The 2-D models should also be capable of accounting for the availability of material for erosion (bed armouring) and updating topography changes (due to erosion/deposition and large-scale bedform development) in the computation of erosion/accretion over the grid.

5) *Morphodynamics of sand ridges on Sable Island Bank and evolution of sand bank bodies.* The morphology and migration of sand ridges and associated large-scale bedforms on SIB is one of the most important engineering issues for offshore energy development and a critical component for understanding the regional sediment transport pattern and evolution of sand bank bodies on the Scotian Shelf. The recently available multibeam technology should be combined with seismic/sidescan surveys to obtain high-resolution data on the morphology, shallow stratigraphy, superimposing relationships, migration rates, and directions of sand ridges and associated bedforms. Instrument packages should be deployed along transects to record the hydrodynamic and sediment transport processes during winter storms. These data should be combined with repetitive multibeam surveys to determine what transport mechanisms control this migration process. These results should also be used to test and improve theoretical models on sand ridge formation (*e.g.*, Huthnance, 1982; Trowbridge, 1995; and Hulscher, 1996). Our knowledge of the regional sediment transport pattern and the genesis and stability of sand ridges, combined with sea-level and glaciation history, will eventually lead to better understanding of the evolution of sand bank bodies on the eastern Canadian shelves.

ACKNOWLEDGMENTS

The authors would like to thank Phil Hill for his vision and effort to organize this special series of "New Developments in Environmental Marine Geoscience." This paper benefited substantially from the internal reviews by Don Forbes and Edward King and from the external reviews by Don Swift, Susan Davidson, and Phil Hill. We also would like to thank Bruce Wile, Bob Murphy, Donny Clattenburg, Gary Grant, Ken Hale, and Phil O'Regan for their field, lab, and drafting support. We appreciate the co-operation and support we received from PanCanadian, Mobil Canada, and Sable Offshore Energy Inc. The funding for the Sediment Dynamics research at GSCA was also provided by the Panel on Energy Research and Development (PERD) through East Coast Offshore Geotechnics Project 12100E01. Geological Survey of Canada Contribution Number 2000164.

REFERENCES

Amos, C.L. and Judge, J.T., 1991, Sediment transport on the eastern Canadian continental shelf: Continental Shelf Research, v. 11, p. 1073-1068.

Amos, C.L. and King, E.L., 1984, Bedforms of the Canadian eastern seaboard: A comparison with global occurrences: Marine Geology, v. 57, p. 167-208.

Amos, C.L., Bowen, A.J., Huntley, D.A. and Lewis, C.F.M., 1988, Ripple generation under the combined influences of waves and currents on the Canadian continental shelf: Continental Shelf Research, v. 8, n.10, p. 1129-1153.

Amos, C.L., Barrie, J.V. and Judge., J.T., 1995, Storm-enhanced sand transport in a macrotidal setting, Queen Charlotte Islands, British Columbia, Canada, *in* Flemming, B.W. and Bartholoma, A., eds., Tidal Signature in Modern and Ancient Sediments: Special Publication, International Association of Sedimentologists, v. 24, p. 53-68.

Anderson, C., 1995, A two-dimensional, time-dependent sediment transport model of Sable Island Bank using SEDTRANS92: Challenger Oceanography Consultant Report, GSC Open File Report 2359.

Arnott, R.W. and Southard, J.B., 1990, Exploratory flow-duct experiments on combined-flow bed configurations, and some implications for interpreting storm-event stratification: Journal of Sedimentary Petrology, v. 60, n. 2, p. 211-219.

Bagnold, R.A., 1956, Flow of cohesionless grains in fluids: Philosophical Transactions of the Royal Society of London, v. A249, p. 235-297.

Bagnold, R.A., 1963, Mechanics of marine sedimentation, *in* Hill, M.N., ed., The Sea: Wiley-Interscience, New York, v. 3, p. 507-527.

Bowen, A.J., 1986, Numerical modelling of sediment transport, *in* Hodgins, D.O., ed., Bottom Sediment Transport-Present Knowledge and Industry Needs: Environmental Studies Research Funds, Ottawa, Report 027, p. 245-293.

Brown, C.B., 1950, *in* Rouse, H., ed., Engineering Hydraulics: John Wiley and Sons, New York, 1039 p.

Cacchione, D.A. and Drake, D.E., 1990, Shelf sediment transport: An overview with applications to the Northern California continental shelf, *in* Le Mehaute, T.B. and Hanes, D.M., eds., The Sea: Wiley-Interscience, v. 9, p. 729-773.

Dalrymple, R.W. and Hoogendoorn, E.L., 1997, Erosion and deposition on migrating shoreface-attached ridges, Sable Island, Eastern Canada: Geoscience Canada, v. 24, p. 25-36.

Drake, D.E. and Cacchione, D.A., 1989, Estimates of the suspended sediment reference concentration (C_a) and resuspension coefficient (γ) from near-bed observations on the California shelf: Continental Shelf Research, v. 9, p. 51-64.

Engelund, F. and Hansen, E., 1967, A monograph on sediment transport in alluvial streams: Teknisk Vorlag, Copenhagen, Denmark, 62 p.

Glenn, S.M. and Grant, W.D., 1987, A suspended sediment stratification correction for combined wave and current flows: Journal of Geophysical Research, v. 92, p. 8244-8264.

Grant W.D. and Madsen, O.S., 1979, Combined wave and current interaction with a rough bottom: Journal of Geophysical Research, v. 84, p. 1797-1808.

Grant, W.D. and Madsen, O.S., 1982, Movable bed roughness in unsteady oscillatory flow: Journal of Geophysical Research, v. 87, p. 469-481.

Grant, W.D. and Madsen, O.S., 1986, The continental shelf bottom boundary layer: Annual Review of Fluid Mechanics, v. 18, p. 265-305.

Hay, A.E. and Sheng, J., 1992. Vertical profiles of suspended sand concentration and size from multifreqency acoustic backscatter: Journal of Geophysical Research, v. 97, p. 15661-15677.

Heathershaw, A.D., 1981, Comparisons of measured and predicted sediment transport rates in tidal currents, *in* Nittrouer, C.A., ed., Sedimentary Dynamics of Continental Shelves: Marine Geology, v. 42, p. 75-104.

Hill, P.S., Nowell, A.R.M. and Jumars, P.A., 1988, Flume evaluation of the relationship between suspended sediment concentration and excess boundary shear stress: Journal of Geophysical Research, v. 93, p. 12499-12509.

Hodgins, D.O., Huntley, D.A., Liam Finn, W.D., Long, B., Drapeau, G. and Bowen, A.J., eds., 1986, Bottom sediment transport - present knowledge and industry needs: Environmental Studies Research Funds, Report 027, Ottawa, 394 p.

Hoogendoorn, E.L. and Dalrymple, R.W., 1986, Morphology, lateral migration and internal structures of shoreface-connected ridges, Sable Island Bank, Nova Scotia, Canada: Geology, v. 14, p. 400 - 403.

Hulscher, S.J.M.H., 1996, Tide-induced large-scale regular bed form patterns in a three-dimensional shallow water model: Journal of Geophysical Research, v. 101, p. 20727-20744.

Huntley, D.A., 1986, Physical concepts of sediment transport on continental shelves, *in* Hodgins, D.O. *et al.*, eds., Bottom Sediment Transport-Present Knowledge and Industry Needs: Environmental Studies Research Funds, Report 027, Ottawa, p. 3-57.

Huthnance, J.M., 1982, On one mechanism forming linear sandbanks: Estuarine and Coastal Marine Science, v. 14, p. 19-99.

Ingersoll, R.W. and Ryan, B.A., 1997, Repetitive surveys to assess sand ridge movement offshore Sable Island: Oceans 97, Proceedings, p. 1377-1393.

Kachel, N. and Smith, J.D., 1986, Geological impact of sediment transporting events on the Washington continental shelf, *in* Knight, R.J. and McLean, J.R., eds., Shelf Sands and Sandstones: Canadian Society of Petroleum Geologists, Memoir 11, p. 145-162.

Li, M.Z., 1994, Direct skin friction measurements and stress partitioning over movable sand ripples: Journal of Geophysical Research, v. 99, p. 791-799.

Li, M.Z. and Amos, C.L., 1995, SED-TRANS92: A sediment transport model for continental shelves: Computers and Geosciences, v. 21, n. 4, p. 533-554.

Li, M.Z. and Amos, C.L., 1998, Predicting ripple geometry and bed roughness under combined waves and currents in a continental shelf environment: Continental Shelf Research, v.18, p.941-970.

Li, M.Z. and Amos, C.L., 1999a, Sheet flow and large wave ripples under combined waves and currents: Their field observation, model prediction and effects on boundary layer dynamics: Continental Shelf Research, v. 19, p. 637-663.

Li, M.Z. and Amos, C.L., 1999b, Field observations of bedforms and sediment transport thresholds of fine sand under combined waves and currents: Marine Geology, v. 158, p. 147-160.

Li, M.Z. and Amos, C.L., 2001, SED-TRANS96: the upgrade and better calibrated sediment transport model for continental shelves: Computers and Geosciences, v. 27, p. 619-645.

Li, M.Z. and Heffler, D.E., 2002, Environmental Marine Geoscience 3. Continental Shelf Sediment Transport Studies in Canada: Theories and Recent Technology Advances: Geoscience Canada, v. 29, p. 35-48.

Li, M.Z., Wright, L.D. and Amos, C.L., 1996, Predicting ripple roughness and sand resuspension under combined flows in a shoreface environment: Marine Geology, v. 130, p. 139-161.

Li, M.Z., Amos, C.L. and Heffler, D.E., 1997, Boundary layer dynamics and sediment transport under storm and non-storm conditions on the Scotian shelf: Marine Geology, v. 141, p.157-181.

Li, M.Z., Amos, C.L. and Heffler, D.E., 1999a, Hydrodynamics and Seabed Stability Observations on Sable Island Bank: A Summary of the Data for 1996/97: Geological Survey of Canada Open File Report 2997.

Li, M.Z., Currie, R., Beaver, D., Girouard, P. and Pledge, P., 1999b, Multibeam Surveys of Sable Island Bank and the Gully Area of Scotian Shelf: Report on Creed Cruise 98-100: Geological Survey of Canada, Atlantic Cruise Report, 44 p.

Nelson, J.M. and J.D. Smith, 1989, Mechanics of flow over ripples and dunes: Journal of Geophysical Research, v. 94, p. 8146-8162.

Nielsen, P., 1981, Dynamics and geometry of wave-generated ripples: Journal of Geophysical Research, v. 86, p. 6467-6472.

Nielsen, P., 1986, Suspended sediment concentrations under waves: Coastal Engineering, v. 10, p. 23-31.

Nielsen, P., 1992, Coastal bottom boundary layers and sediment transport: Advanced Series on Ocean Engineering - v. 4, World Scientific, Singapore, 324 p.

Nittrouer, C.A., 1999, STRATAFORM: Overview of its design and synthesis of its results: Marine Geology, v. 154, p. 3-12.

Nittrouer, C.A. and Wright, L.D., 1994, Transport of particles across continental shelves: Reviews of Geophysics, v. 32, p. 85-113.

Rouse, H., 1937, Modern conceptions of the mechanics of turbulence: American Society of Civil Engineers, Transactions, v. 102.

Smith, J.D., 1977, Modelling of sediment transport on continental shelves, *in* Goldberg, E.D., McCave, I.N., O'Brien, J.J. and Steele, J.H., eds., The Sea: Wiley-Interscience, New York, v. 6, p.539-576.

Smith, J.D. and McLean, S.R., 1977, Spatially averaged flow over a wavy surface: Journal of Geophysical Research, v. 82, p. 1735-1746.

Sternberg, R.W., 1972, Predicting initial motion and bedload transport of sediment particles in the shallow marine environment, *in* Swift, D.J.P., Duane, D.B. and Pilkey, O.H., eds., Shelf Sediment Transport, Process and Pattern: Dowden, Hutchinson & Ross, p. 61-83.

Trowbridge, J.H., 1995, A mechanism for the formation and maintenance of shore-oblique sand ridges on storm-dominated shelves: Journal of Geophysical Research, v. 100, p. 16071-16086.

van Rijn, L.C., Nieuwjaar, M.W.C., Van der Kaay, T., Nap, E. and van Kampen, A., 1993, Transport of fine sands by currents and waves: Journal of Waterway, Port, Coastal and Oceanic Engineering, ASCE, v. 119, n. 2, p. 123-143.

Vincent, C.E., Hanes, D.M. and Bowen, A.J., 1991, Acoustic measurements of suspended sand on the shoreface and the control of concentration by bed roughness: Marine Geology, v. 96, p. 1-18.

Wiberg, P.L. and Nelson, J.M., 1992, Unidirectional flow over asymmetric and symmetric ripples: Journal of Geophysical Research, v. 97, p. 12745-12761.

Wiberg, P.L. and D.M. Rubin, 1989, Bed roughness produced by saltating sediment. Journal of Geophysical Research, v. 94, p. 5011-5016.

Wiberg, P.L. and Smith, J.D., 1983, A comparison of field data and theoretical models for wave-current interactions at the bed on the continental shelf: Continental Shelf Research, v. 2, p. 147-162.

Wilson, K.C., 1988, Mobile-bed friction at high shear stress: Journal of Hydraulic Engineering, ASCE, v. 115, p. 825-830.

Wright, L.D., 1989, Benthic boundary layers of estuarine and coastal environments: Reviews in Aquatic Science, v. 1, p. 75-95.

Wright, L.D., 1993, Micromorphodynamics of the inner continental shelf: A Middle Atlantic Bight case study: Journal of Coastal Research, Special Issue 15, p. 93-124.

Yalin, M.S., 1963, An expression for bedload transportation: Journal of the Hydraulics Division, Proceedings ASCE, v. 89, HY3, p. 221-250.

Accepted as revised 19 December 2001